AGU PUBLICATIONS

JGR

Journal of Geophysical Research: Oceans

RESEARCH ARTICLE

10.1002/2016JC011831

Key Points:
- A distinct change in the seasonal evolution of ice albedo at the SHEBA geolocations has occurred since 2007
- Summer evolution of ice albedo matched ice surface melting and ponding well at basin scale
- A positive Arctic Dipole Anomaly might enhance the ice-albedo feedback in the Pacific sector of Arctic Ocean

Correspondence to:
R. Lei,
leiruibo@pric.org.cn

Citation:
Lei, R., X. Tian-Kunze, M. Leppäranta, J. Wang, L. Kaleschke, and Z. Zhang (2016), Changes in summer sea ice, albedo, and portioning of surface solar radiation in the Pacific sector of Arctic Ocean during 1982–2009, *J. Geophys. Res. Oceans*, *121*, 5470–5486, doi:10.1002/2016JC011831.

Received 23 MAR 2016
Accepted 6 JUL 2016
Accepted article online 11 JUL 2016
Published online 5 AUG 2016

Changes in summer sea ice, albedo, and portioning of surface solar radiation in the Pacific sector of Arctic Ocean during 1982–2009

Ruibo Lei[1], Xiangshan Tian-Kunze[2], Matti Leppäranta[3], Jia Wang[4], Lars Kaleschke[2], and Zhanhai Zhang[1]

[1]Key Laboratory for Polar Science of the State Oceanic Administration, Polar Research Institute of China, Shanghai, China, [2]Institute of Oceanography, University of Hamburg, Hamburg, Germany, [3]Department of Physics, University of Helsinki, Helsinki, Finland, [4]NOAA Great Lakes Environmental Research Laboratory, Ann Arbor, Michigan, USA

Abstract SSM/I sea ice concentration and CLARA black-sky composite albedo were used to estimate sea ice albedo in the region 70°N–82°N, 130°W–180°W. The long-term trends and seasonal evolutions of ice concentration, composite albedo, and ice albedo were then obtained. In July–August 1982–2009, the linear trend of the composite albedo and the ice albedo was −0.069 and −0.046 units per decade, respectively. During 1 June to 19 August, melting of sea ice resulted in an increase of solar heat input to the ice-ocean system by 282 MJ·m^{-2} from 1982 to 2009. However, because of the counter-balancing effects of the loss of sea ice area and the enhanced ice surface melting, the trend of solar heat input to the ice was insignificant. The summer evolution of ice albedo matched the ice surface melting and ponding well at basin scale. The ice albedo showed a large difference between the multiyear and first-year ice because the latter melted completely by the end of a melt season. At the SHEBA geolocations, a distinct change in the ice albedo has occurred since 2007, because most of the multiyear ice has been replaced by first-year ice. A positive polarity in the Arctic Dipole Anomaly could be partly responsible for the rapid loss of summer ice within the study region in the recent years by bringing warmer air masses from the south and advecting more ice toward the north. Both these effects would enhance ice-albedo feedback.

1. Introduction

Although the rate of global warming has slowed during the last decade [*Kosaka and Xie*, 2013], Arctic air temperature has continued to increase at more than twice the global rate, which is a phenomenon referred to as Arctic Amplification [*Serreze and Barry*, 2011]. Reduced summer albedo caused by sea ice retreat and surface melting is one of major causes of Arctic Amplification [*Screen and Simmonds*, 2010; *Pithan and Mauritsen*, 2014]. The darkening of the Arctic Ocean surface, resulting from the decrease of albedo, introduced an additional 6.4 ± 0.9 W/m^2 of annual average solar heat input into the ocean from 1979 to 2011[*Pistone et al.*, 2014]. Averaged over the globe, this corresponds to a forcing equal to 25% of that caused by increased emissions of CO_2 [*Pistone et al.*, 2014].

Melt ponds contribute to ice-albedo feedback because they reduce the albedo [*Perovich et al.*, 2002; *Lu et al.*, 2016] and accelerate sea ice fragmentation by weakening its mechanical strength [*Timco and Johnston*, 2002]. The melt pond fraction in the early melt season has been used to predict the September Arctic sea ice extent because of the positive feedback mechanism [*Schröder et al.*, 2014]. Because of the different surface characteristics and ponding processes, first-year sea ice has different seasonal evolution of albedo compared with multiyear ice [*Perovich et al.*, 2002; *Perovich and Polashenski*, 2012; *Webster et al.*, 2015]. Thus, rapid depletion of multiyear ice in the Arctic Ocean [*Maslanik et al.*, 2011] would lead to significant change in basin-scale albedo. A proper parameterization of the albedo of ice-covered oceans is essential for the treatment of ice-albedo feedback in climate models [*Liu et al.*, 2007]. The composite albedo of an ice-covered ocean can be defined by the area fractions and albedos of sea ice and open water. In contrast to sea ice, open water albedo has a narrow range [*Pegau and Paulson*, 2001] and therefore, sea ice albedo is the critical variable for the parameterization of the composite albedo.

The most significant decline of summer Arctic sea ice extent has occurred in the Pacific sector from the Beaufort Sea to the East Siberian Sea [*Xia et al*., 2014]. Sea ice surface melting in the Beaufort Sea remarkably exceeded that of the central Arctic Ocean [*Perovich and Richter-Menge*, 2016]. Consequently, both the decrease in the regional composite albedo and the increase in the solar radiation transmittance through the ice in this sector were much more distinct than in other Arctic sectors [*Nicolaus et al*., 2012; *Arndt and Nicolaus*, 2014; *Pistone et al*., 2014]. Therefore, to analyze the change in Arctic sea ice albedo, this study focused on the region of 130°W–180°W in the Pacific sector.

In situ observations are very important to characterize the ice-albedo feedback mechanism [e.g., *Perovich et al*., 2002; *C. Wang et al*., 2014]. However, from a large-scale modeling or for a climate perspective, the understanding of evolution of floe-scale albedo is not enough. For most parameterizations of sea ice albedo which have been established based on in situ measurements [e.g., *Perovich et al*., 2007a; *Perovich and Polashenski*, 2012], their upscale applicability has not been fully validated because of the lack of basin-scale measurements. This highlights the value of satellite remote sensing observations. Using albedo data from the Clouds and Earth's Radiant Energy System (CERES) in combination with sea ice concentration derived from passive microwave measurements, estimates of sea ice albedo have been produced [*Pistone et al*., 2014]. However, the CERES albedo was only available from 2000 to 2011, which prevents us from obtaining the long-term changes. The surface black-sky albedo of Earth, i.e., the directional-hemispherical reflectance, has been retrieved using the measurements of the Advanced Very High Resolution Radiometer (AVHRR) by the Satellite Application Facility on Climate Monitoring (CMSAF) project. These data comprise part of the CMSAF clouds, Albedo and Radiation first release product family (CLARA-A1-SAL) [*Riihelä et al*., 2013a]. The CLARA albedo data set is available during spring-summer 1982–2009, which permits the exploration of both seasonal and long-term changes. The long-term change in the sea ice albedo for the entire Arctic Ocean has been obtained and analyzed using this data set by *Riihelä et al*. [2013b]. As an extension and complement, this study focused mainly on the seasonal evolution of sea ice albedo. At a local scale, seasonal evolution of ice albedo can be closely related to ice surface melting and ponding processes [*Perovich et al*., 2002; *Perovich and Polashenski*, 2012]. However, these relationships at basin scale have not been sufficiently discussed. The onsets of ice surface melt and refreezing can be determined by satellite passive microwave measurements [*Markus et al*., 2009]. The melt pond fraction can be retrieved from the Moderate Resolution Imaging Spectroradiometer (MODIS) optical measurements [*Rösel et al*., 2012]. Both data benefit exploring the relationship between ice albedo and ice surface melting at basin scale.

The determination of partitioning of surface solar radiation is crucial for thoroughly understanding the interactions of solar radiation with the ice cover [*Wang et al*., 2016]. Using the data of sea ice concentration and albedo, surface solar radiation can be classified into the part reflected by the Earth's surface and those inputs to the sea ice and open water separately [*Perovich et al*., 2007b,2011]. In previous studies, this classification was determined using only the ice albedo parameterization derived from the measurements during the Surface Heat Budget of the Arctic (SHEBA) campaign. However, it can be expected that there would be some differences between floe-scale and basin-scale sea ice albedo. In this study, surface incident solar radiation was obtained from daily values of the European Centre for Medium-Range Weather Forecasts (ECMWF) ERA-Interim reanalyses. The satellite-derived ice concentration and albedo were used to estimate the portioning of surface solar radiation. The poleward gradient of the ice albedo and surface radiation portioning from the marginal ice zone to the pack ice zone was analyzed, which can be related to the difference in albedo between first-year and multiyear ice, and to the poleward gradients of ice surface ponding and open water fraction.

In general, the main objectives of this study are to quantify the long-term and seasonal changes in Arctic sea ice albedo and their relations to the sea ice surface melting and ponding at basin scale, which can provide new understanding for ice albedo parameterizations used in numerical models.

2. Data and Methods

2.1. Sea Ice Concentration and Albedo

The CLARA albedo has been determined in the clear-sky pixels after cloud masking and correction for topographic, anisotropic, and atmospheric effects in the observed surface radiance. This albedo is taken across a broad band of wavelengths of 250–2500 nm for snow-free surfaces and 350–2800 nm for snow surfaces

[*Riihelä et al*., 2013a], i.e., almost covering the entire spectral range of incident solar radiation. The data used here were the Arctic subset, with 25 km resolution provided on an equal-area polar grid. The CLARA data set is available from 1982 to 2009, providing products every 5 days throughout the period that receives solar insolation. It contains some pixels with missing data due to cloud effects, and therefore spatial-temporal gap filling was conducted using the method of *Riihelä et al*. [2013b]. Pixels with missing values constitute about 2.5% of the data obtained in our study region throughout the entire period. To explore the poleward gradient of ice albedo, the study region was divided into three subregions: 70°N–74°N, 74°N–78°N, and 78°N–82°N. In summer, the region 70°N–74°N can be defined as the marginal ice zone (MIZ) because sea ice in this region would melt completely for most years, while the region 78°N–82°N can be defined as the pack ice zone (PIZ) because the ice edge would not shrink into this region for most years [*Xia et al*., 2014]. The region 74°N–78°N is the transition zone. CLARA albedo is available in summer only until 3 September, 24 August, and 19 August for these three subregions because of the limitations of satellite viewing angle and sun zenith angle. According to the available period of CLARA albedo, the summer period is henceforth defined as May–August, if no other definition is offered.

Time series of the data from the Defense Meteorological Satellite Program Special Sensor Microwave/Imager (SSM/I), and both its predecessor (Scanning Multichannel Microwave Radiometer, SMMR) and its successor (Special Sensor Microwave Imager Sounders, SSMIS), have provided consistent information on sea ice concentration since 1979. Here we used the daily ice concentration retrieved using the Bootstrap (BST) algorithm [*Comiso*, 2000], which has a spatial resolution of 25 $\times$ 25 km^2 and is called as the SSM/I BST ice concentration thereafter. Comparison to summer ship-based visual observations shows that both the bias and the error standard deviation of the SSM/I BST ice concentration are smaller or comparable with those obtained from the NASA/Team or NASA/Team 2 algorithm [*Andersen et al*., 2007; *Beitsch et al*., 2015]. The albedo (α) of a pixel comprising open water and sea ice can be defined as:

$$\alpha = C_i \alpha_i + C_w \alpha_w, \tag{1}$$

where C_i and C_w are the area fractions of sea ice and open water, and α_i and α_w are their albedos, respectively. Sea ice albedo can be estimated using the satellite-derived data of composite albedo and ice concentration because the albedo of open water can be set to a constant value of 0.07 [*Pegau and Paulson*, 2001]. To estimate sea ice albedo, only those pixels with an ice concentration of $>$15% were considered. The 5 day sampling window provides more cloud-free pixels for the retrieval of CLARA albedo and normalizes the influences of variations in sun zenith angle. However, this leads to the different sampling frequency between CLARA albedo and sea ice concentration. To calculate sea ice albedo, we used the daily sea ice concentration obtained from the middle day of each sampling period of CLARA albedo. Climatological averages of summer sea ice concentration, composite albedo, and sea ice albedo during 1982–2009 are shown in Figure 1.

Comprehensive in situ observations of the sea ice albedo were conducted during the SHEBA campaign [*Perovich et al*., 2002]. The aerial observation showed that the melt pond fraction obtained from the 200 m albedo survey line of SHEBA has a close seasonal evolution with those of a local region of 50 $\times$ 50 km^2 [*Perovich et al*., 2002]. Therefore, the albedo averaged from this survey line has a high local representativeness. To assess the plausibility of the satellite-derived ice albedo, the data obtained at the grid cell containing SHEBA coordinates were compared with the SHEBA data. To determine the long-term change, the satellite-derived ice albedo obtained from four nearest pixels on a given day during 1982–2009 was spatially interpolated into the SHEBA locations using the inverse-distance weighting method. For the analysis of seasonal evolution, we focused on the period 1 May to 3 September because of the limitation of the CLARA data. The in situ measurements showed that sea ice albedo was nearly constant prior to May but then had large seasonal changes because of the formation, evolution, and refreezing of melt ponds [*Perovich et al*., 2002; *Perovich and Polashenski*, 2012].

2.2. Melt Season and Melt Ponds

Based on the SSM/I brightness temperatures, *Markus et al*. [2009] defined four stages for the ice surface during the melting season: early melt (earliest observed melting), full melt (melting throughout), early freezeup (earliest observed freezing), and full freezeup (freezing throughout). The period between the full melt and early freezeup can be considered as the season of uninterrupted melt. We used this data set to characterize the relationship between the seasonal evolution of ice albedo and ice surface melting.

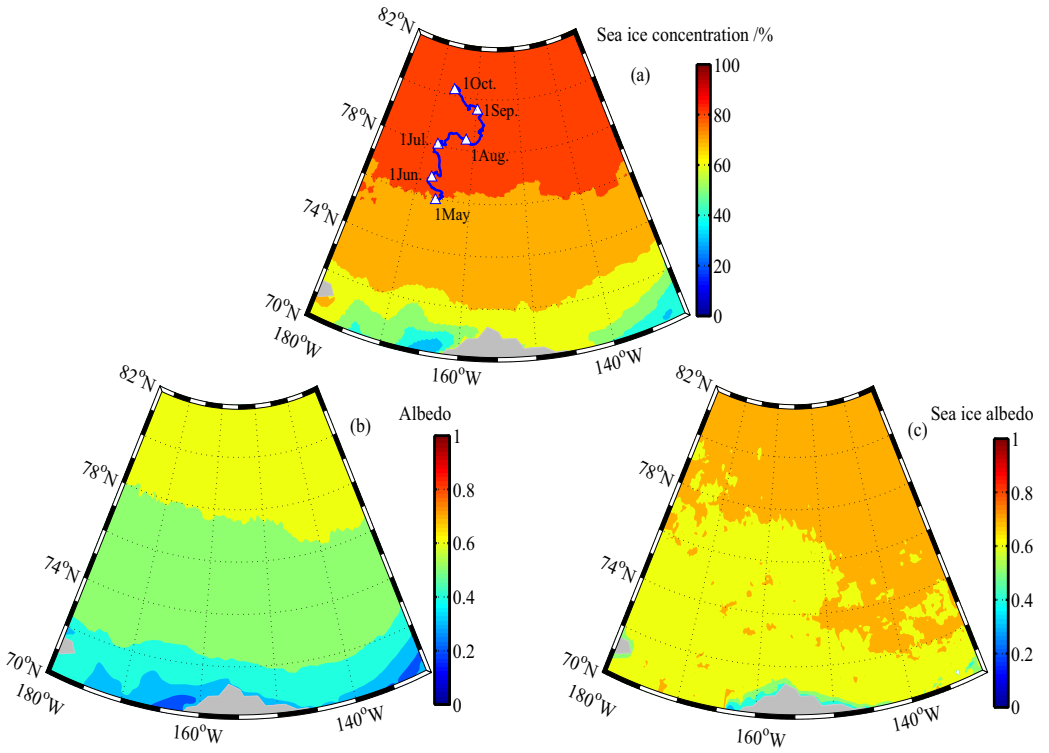

Figure 1. Climatological averages of (a) sea ice concentration, (b) composite albedo, and (c) sea ice albedo from 1 May to 19 August 1982–2009. Also shown is the track of the SHEBA campaign (blue line in Figure 1a).

The melt pond fraction is defined as the area ratio between melt pond and sea ice. Melt pond coverage can be obtained by scaling this fraction with the ice concentration. The melt pond fraction can be derived from the level 3 MODIS surface reflectance product using a spectral unmixing algorithm [*Rösel et al*., 2012]. This product, available every 8 days from 18 May to 7 September (2000–2011), was used to determine the relationship between the seasonal evolution of ice albedo and ice surface ponding. Since this data set is a composite of selected could-free pixels, to avoid low data quality, we selected only grid cells, which contain more than 50% cloud-free cases during one sampling period. After this filtration, pixels with missing values constitute about 10% in our study region throughout the entire study period. To fill up the gaps of small area (less than 12.5 km^2) caused by cloud filtering, we use the corresponding pixel from days before and after the relevant data as *Rösel et al*. [2012]. Otherwise, the gaps of larger areas are neglected and masked, which constitute about 5% of the data. The difference of sampling frequency between MODIS melt pond and CLARA albedo would not be considered here, because the seasonal evolutions only will be qualitatively compared between two.

2.3. Reanalyzed Atmospheric Data

Incident solar radiation was obtained from the ECMWF ERA-Interim reanalysis data on a 1.5° regular grid. Combined with the satellite-derived sea ice albedo and concentration, the partitioning of surface solar radiation, including components of reflected by and input to sea ice and open water, could be obtained. Prior to the calculation, the ERA reanalysis data obtained from the regular grids are reprojected into the equal-area polar grids to match the data of albedo and sea ice concentration. The summer (May-August) NCEP/NCAR Reanalysis 2 surface-level pressure data north of 70°N were used to derive the empirical orthogonal function (EOF) modes. The Arctic Oscillation (AO) and the Dipole Anomaly (DA) correspond to the first and second leading modes of the EOF, respectively [*Wang and Ikeda*, 2000]. Here we have analyzed the empirical relationships between the long-term change in sea ice and its albedo and the summer AO/DA indices. This allowed us to explore the response of sea ice change to the atmospheric circulation.

The correlation between the variables was determined using the Pearson correlation analysis, while the statistical significance of all long-term trends was evaluated using a two-tailed Student's *t* test.

Table 1. Autocorrelation Coefficients of Time Series of Sea Ice Concentration, Composite Albedo, and Sea Ice Albedo for Three Latitude Zones and Two Subperiods in 1982–2009[a]

Latitude Zone	Subperiod	Sea Ice Concentration	Composite Albedo	Sea Ice Albedo
70°N–74°N	May to Jun	0.52**	0.74***	0.79***
	1 Jul to 3 Sep	0.67***	0.77***	0.83***
74°N–78°N	May to Jun	0.57**	0.82***	0.76***
	1 Jul to 24 Aug	0.8***	0.86***	0.71***
78°N–82°N	May to Jun	0.43*	0.58**	0.58**
	1 Jul to 19 Aug	0.58**	0.66***	0.51**

[a]Significance levels are shown as $p < 0.001$ (***), $p < 0.01$ (**), and $p < 0.05$ (*).

3. Results

3.1. Long-Term Changes in Sea Ice Concentration and Albedo

In both early summer (May–June) and late summer (July–August), sea ice concentration, composite albedo, and sea ice albedo all showed significant declining trends during 1982–2009 (Table 1). However, the long-term trends for these variables had different seasonal patterns. The declining trend of sea ice concentration in late summer was stronger than in early summer, because sea ice concentration maintained relatively large values in the early summer of most years. The long-term average ice concentration during early summer in the region 70°N–74°N was 78%. In contrast, the long-term change of sea ice albedo in early summer was similar to late summer.

The long-term trend of sea ice loss and the decrease in the regional composite albedo in the region 74°N–78°N were stronger than in lower or higher latitudes. In lower latitudes, the seasonal retreat of sea ice was remarkable, even in the early years, whereas in higher latitudes, sea ice concentration remained relatively high into late summer, even until recent years. Compared with sea ice concentration, the long-term change in sea ice albedo showed different spatial dependence; i.e., it was stronger in lower latitudes. This could be attributed to the fact that the trend toward a longer melt season was stronger in the region 70°N–74°N than in higher latitudes.

The Pearson correlation analysis (Table 2) showed that the early summer long-term declining trend of the regional composite albedo depends more strongly on the decrease of the sea ice albedo than on the decline of sea ice concentration. This is because the decrease in sea ice albedo is already apparent in mid-May, while sea ice concentration begins to decrease considerably later. In contrast, in late summer, the decline of sea ice concentration provides a comparable or larger contribution to the long-term trend of composite albedo, because the decline of sea ice concentration reaches its fastest rate in July–August. During 1 July to 19 August, the average sea ice concentration within the study region decreased by about 25% from 1982 to 2009. The average sea ice albedo decreased by about 0.12 or 20% (Figure 2). The joint contribution resulted in a decrease in the regional composite albedo by about 0.19 or 38%. The trends of regional composite albedo and sea ice albedo were about twice as large in magnitude relative to those of the entire Arctic Ocean [*Riihelä et al*., 2013b].

3.2. Seasonal Evolution of Sea Ice Albedo

From the 1982–2009 climatology (Figure 3), we found that sea ice concentration remained relatively large (>88%) until 10 June. From then onward, it started to decrease gradually. Sea ice concentration reached a stable level of about 60% by mid-August. The decrease in sea ice albedo commenced earlier, i.e., on about 21 May. This decrease can be divided into two phases. In the first phase that lasted until early July, sea ice albedo decreased rapidly from 0.85 to 0.60. From early July to the end of August, sea ice albedo decreased

Table 2. Correlation Coefficients Between Regional Albedo (α) and Sea Ice Concentration (C_i) or Sea Ice Albedo (α_i) for Three Latitude Zones and Two Subperiods in 1982–2009[a]

	70°N–74°N		74°N–78°N		78°N–82°N	
	C_i	α_i	C_i	α_i	C_i	α_i
α (May–Jun)	0.867	0.964	0.732	0.884	0.733	0.951
α (Jul–Aug)	0.967	0.937	0.952	0.846	0.845	0.829

[a]All correlations are significant at the confidence level of 0.001.

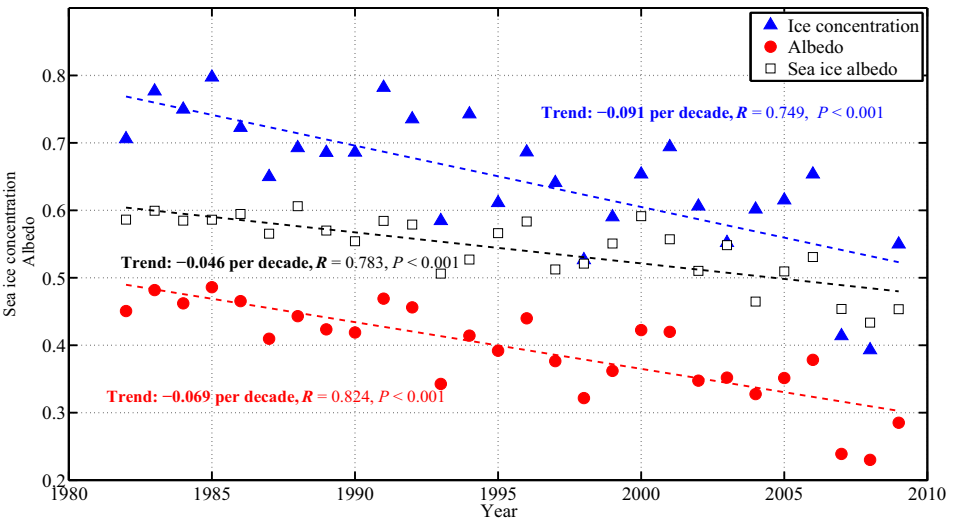

Figure 2. Long-term trends of sea ice concentration, composite albedo, and sea ice albedo averaged during 1 July to 19 August in the study region. Also shown are the correlation coefficients and confidence levels of the linear trends.

relatively slowly, because of the counteraction between the continued ice melt in low latitudes and the refreezing in high latitudes, which could be supported by the difference of the changes in sea ice albedo during this period among three subregions (will be discussed later). The regional composite albedo decreased more rapidly because of the loss of sea ice area.

By comparing the remotely sensed ice albedo with the SHEBA in situ data (Figure 4a), we found that both albedos showed similar summer evolutions, i.e., starting to decrease gradually from about 20 May onward, reaching an annual minimum by about mid-July, and finally starting to increase again from about 20 July onward. The ice albedo derived from the remote sensing data was slightly larger than the average of the SHEBA outcome. Most of in situ SHEBA albedo was obtained on cloudy days [*Perovich et al*., 2002]. The albedo is 0.077 and 0.012 greater under overcast than under clear sky for snow-covered ice and melt pond, respectively [*Grenfell and Perovich*, 1984]. Taking into account the influence of clouds and assuming a melt pond fraction of 25%, the overcast albedo is about 0.06 larger than the clear-sky albedo. According to *Pistone et al*. [2014], the all-sky albedo can be approximately estimated as:

$$\alpha_{as} = (1 - C)\alpha_{cs} + C\alpha_{cld}, \tag{2}$$

where α_{as}, α_{cs} and α_{cld} are all-sky, clear-sky and overcast albedos, and C is the cloud fraction. Using the climatology of Arctic cloud fraction of 75% in June–August obtained from satellite observations during 1982–

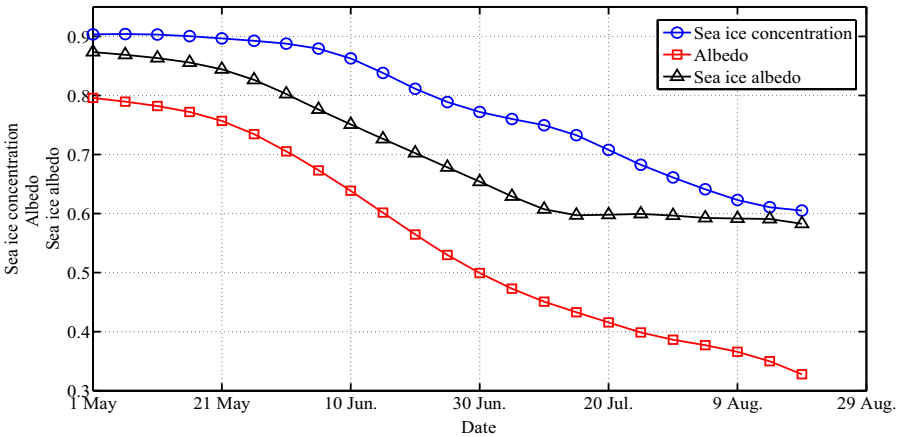

Figure 3. Seasonal evolutions of sea ice concentration, composite albedo, and sea ice albedo within the study region from 1 May to 19 August averaged over 1982–2009.

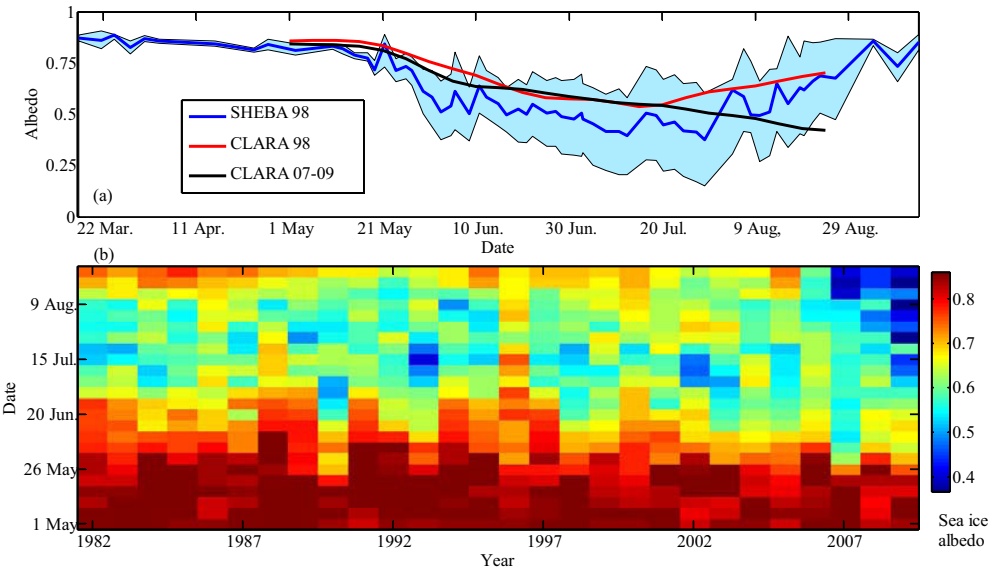

Figure 4. (a) Seasonal evolution of SHEBA sea ice albedo and those estimated using the satellite data in 1998 and averaged over 2007–2009 at the SHEBA coordinates; the blue shading indicates one standard deviation of the SHEBA spatial variability along the 200 m survey line. (b) Seasonal evolution of sea ice albedo estimated using the satellite data of 1982–2009 at the SHEBA coordinates.

2004 [*Wang et al*., 2012], the all-sky albedo is about 0.045 greater than the clear-sky albedo. However, even considering such adjustments the remote sensing albedo was still within the one standard deviation of the SHEBA spatial variability along the 200 m survey line. Furthermore, aerial measurements showed that although the summer evolution of melt pond fraction obtained from the SHEBA 200 m albedo survey line was comparable with that obtained from the local region of 50 × 50 km^2, the absolute magnitude of melt pond fraction in mid-July obtained from the survey line was 10% less than that obtained from the local region [*Perovich et al*., 2002], which implies a difference of about 0.04 for the albedo of composite surface of snow-covered ice and melt pond. This can partly explain why remotely sensed ice albedo obtained from four nearest pixels (∼50 × 50 km^2) was slightly larger than the average SHEBA albedo.

To obtain the long-term change of the summer sea ice albedo, we also interpolated the remotely sensed ice albedo of other years, using the data obtained from four nearest pixels, into the SHEBA locations (Figure 4b). Prior to 2007, ice albedo showed a similar seasonal evolution. However, an obvious change, which occurred after 2007, was the absence of a distinct increase of the ice albedo in late August. This can be attributed to the fact that most sea ice at the SHEBA locations would melt completely by the end of summer. Field experiments have shown that the albedo of first-year ice would decrease to about 0.2 prior to its complete melt [*Perovich and Polashenski*, 2012]. The refreezing of open water in autumn would be delayed compared with the survived multiyear ice.

A significant anomaly in the melt pond fraction at the beginning of the melt season in June 2007 was observed [*Rösel and Kaleschke*, 2012], the subsequent value of which was above the long-term average throughout the entire summer. This anomaly in melt pond fraction was more pronounced in the Pacific sector from the Beaufort Sea to the East Siberian Sea [*Rösel and Kaleschke*, 2012]. Consequently, the June–August average of sea ice albedo interpolated into the SHEBA coordinates was 0.54 in 2007, much smaller than the average value of 0.62 during 1982–2009. This would have partly contributed to the dramatic retreat of sea ice during the summer of 2007.

The SSM/I ice concentration data illuminates that more than 70% of the sea ice in the region 70°N–74°N in the study area melts completely by the end of the melt season, while more than 80% of the sea ice in the region 78°N–82°N survives the summer, as shown in Figure 5. Therefore, most of the sea ice in the region 70°N–74°N can be classified as first-year ice, whereas most of the sea ice in the region 78°N–82°N can be classified as multiyear ice. To compare sea ice albedo with ice surface ponding, only data from 2000 to 2009 were used, because the MODIS-derived melt pond fraction was available only after 2000. As shown in Figure 6, sea ice albedo in the region 70°N–74°N started to decrease from about mid-May, when the ice surface

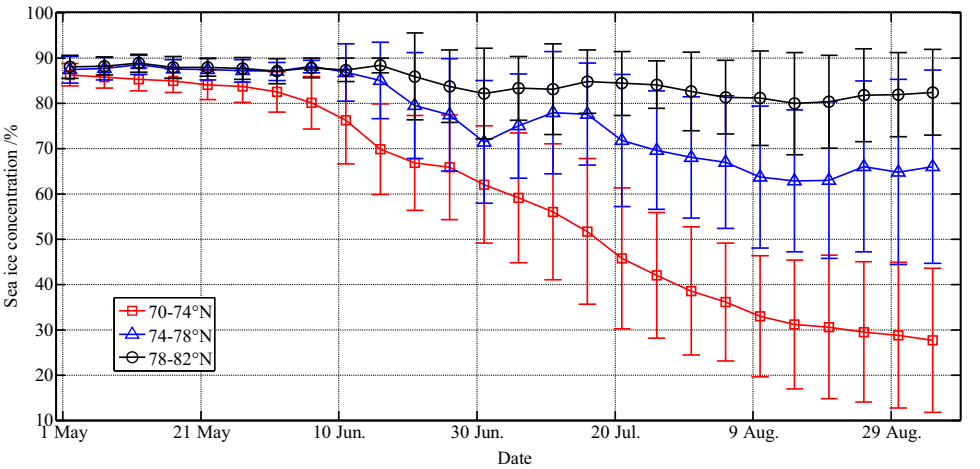

Figure 5. Summer evolution of the averages and standard deviations of sea ice concentration in three subregions over 1982–2009.

melt commenced. From then onto the end of August, ice albedo decreased rapidly from about 0.85 to 0.30 in conjunction with snow melting and the formation and evolution of melt ponds. From mid-May to mid-June, melt pond fraction increased from less than 10% to about 28%, causing a rapid decrease in sea ice albedo. However, from late June onward, although melt pond fraction decreased gradually, sea ice albedo continued to decline. Therefore, the decrease in melt pond fraction could be attributed to the disintegration of floes in this region, but not to the refreezing of melt ponds.

Based on the observation of seasonal landfast ice in Barrow, Alaska, the seasonal evolution of ice albedo can be divided into seven phases: dry snow, melting snow, pond formation, pond drainage, pond evolution, open water, and freezeup [*Perovich and Polashenski*, 2012] (call as Parameterization-2012 thereafter). After the formation of melt ponds, the expansion and interconnection of a brine channel system within the sea

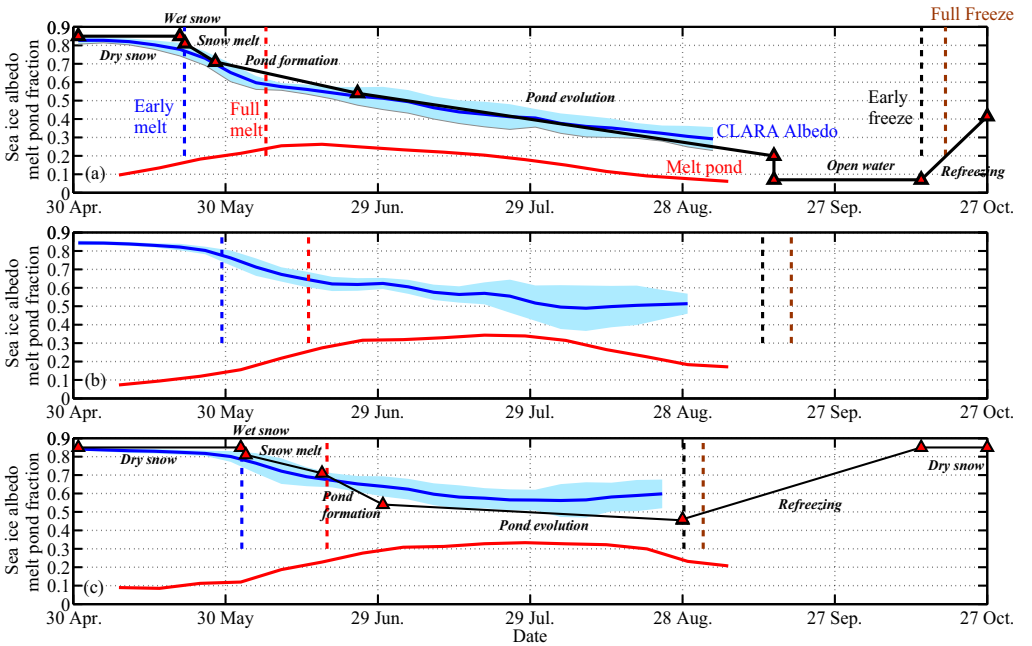

Figure 6. Seasonal evolution of satellite-derived ice albedo, parameterized ice albedo and melt pond fraction, and onsets of ice surface early melt, full melt, early freezeup, and full freezeup averaged over 2000–2009 in the regions (a) 70°N–74°N, (b) 74°N–78°N, and (c) 78°N–82°N. Blue shading denotes the standard deviation. The parameterized ice albedos (black line with red triangles) shown in Figures 6a and 6c were obtained using the adjusted parameterizations for first-year and multiyear ice, respectively.

Table 3. Adjusted Parameterizations for the Albedo of First-Year Ice and Multiyear Ice

Phase	Adjusted Parameterization-2012 for First-Year Ice	Adjusted Parameterization-2007 for Multiyear Ice
Dry snow	0.85	0.85
Wet snow after melt onset	0.81	0.81
Snow melts and changes to bare ice	Decrease linearly to 0.71 within 6 days	Decrease linearly to 0.71 within 15 days
Melt pond formation	Decrease linearly to 0.54 within 28 days	Decrease linearly to 0.54 within 12 days
Melt pond evolution	Decrease by 0.0166 per day until it reaches 0.2	Decrease by 0.0145 per day
Thin ice melts completely	Drop in a single day to 0.07	N/A
After the onset of freezeup in autumn	Increase by 0.025 per day until the maximum of 0.85	Increase by 0.0082 per day until the maximum of 0.85

ice induces surface water drainage and reduces the pond area [*Grenfell and Perovich*, 2004]. However, because of the large spatial and interannual variability, no episodic decrease in melt pond fraction could be identified from the satellite-derived results as shown in Figure 6. Therefore, we adjusted the Parameterization-2012 by neglecting pond drainage. In addition, because this parameterization was based on observations in a relatively southerly region (71°N), we halved the rate of decline of ice albedo due to the formation and evolution of melt ponds and tripled the rate of increase of ice albedo due to freezeup in autumn. The adjusted Parameterization-2012 is described in Table 3. The seasonal evolution and value of sea ice albedo determined by the adjusted Parameterization-2012 was close to the satellite-derived value with maximal deviations of <0.05 (Figure 6a). Here it is noted that we have no satellite-derived data to validate the parameterized ice albedo in the phases of complete melting and freezeup.

The decrease in sea ice albedo in higher latitudes was also strongly related to the onsets of ice surface melting and ponding. Because of the poleward delay of the onset in ice surface melting, the onset of the increase in melt pond coverage and the decrease in ice albedo showed delays in the regions of 74°N–78°N and 78°N–82°N compared with 70°N–74°N. In the region 78°N–82°N, sea ice albedo reached an annual minimum by mid-August, and then it showed an inconspicuous increase with the decrease in melt pond fraction. We infer that the regime resulting in the decrease in the pond area in higher latitudes from late August onward was the surface refreezing, caused by low air temperatures. It was different from the regime for the lower latitudes, which was mainly attributed to the disintegration of floe as mentioned above.

Here we also provide a simple parameterization to describe the summer evolution of sea ice albedo in the region 78°N–82°N, which has been adjusted in comparison with the parameterization based on the SHEBA measurements of multiyear ice [*Perovich et al*., 2007a] (called as Parameterization-2007 thereafter). Figure 4 shows that the rate of decline of the satellite-derived ice albedo was smaller than that of the SHEBA in situ data during the formation and evolution of melt ponds. Therefore, we adjusted the decline rate of the ice albedo during these phases to be half that of Parameterization-2007. The adjusted parameterization for multiyear ice albedo is described in Table 3. Ice albedo determined by this parameterization was also very close to the satellite-derived data with maximal deviations of <0.12 (Figure 6c).

3.3. Ice-Albedo Feedback

Ice-albedo feedback is positive and it can be described as the decrease of albedo that leads to increased absorption of solar radiation and strengthening of the ice melting, which further reduces the albedo [*J. Wang et al*., 2014]. In addition to the forcing of surface air temperature, the onset of ice surface melting is also modulated by snow accumulation during winter and the topography of the ice surface [*Eicken et al*., 2004; *Grenfell and Perovich*, 2004]. In our study region, the long-term trend of the onset of ice surface melting was statistically insignificant (Figure 7a). This can be partly explained by that the main factors influencing the onset of ice surface melt, especially snow accumulation, are independent in the consecutive summers, although the thinning of sea ice was continuing. Furthermore, satellite observation shows that the spring (March–May) cloud fraction increased by 2.3% per decade from 1982 to 2004 [*Wang et al*., 2012]. The increase of spring cloud would counteract partly the surface warming and hamper early onset of ice surface melt through reducing the incident radiation, which has been defined as the cloud cooling effect by *Wang et al*. [2012]. Consequently, the declining trend of ice albedo during the melt season was attributed mainly to the enhanced melting of the ice surface during summer rather than the early onset of melting.

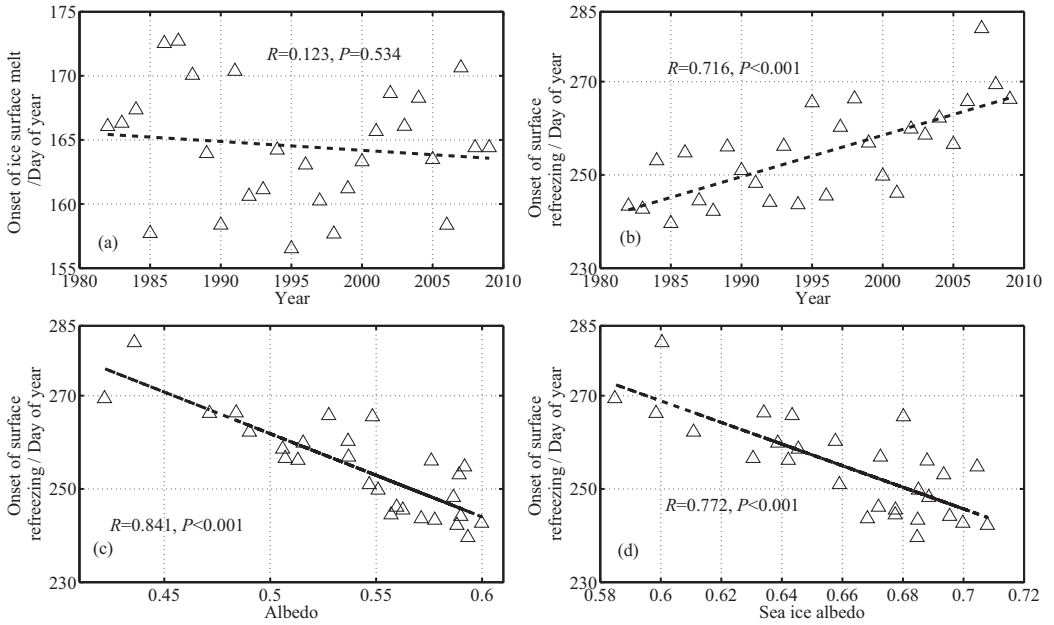

Figure 7. (a and b) Trends of the onsets of ice surface full melt and early freezing from 1982 to 2009, and (c and d) linear regression of the onset of ice surface early freezing against regional composite albedo and sea ice albedo averaged from 1 May to 19 August 1982–2009. Also shown are the correlation coefficients and confidence levels of the linear regressions.

In contrast, the long-term trend of ice surface freezeup was statistically significant at the 99.9% confidence level (Figure 7b), which can be attributed that the accumulated solar radiation within the ice-ocean system during the melt season would enhance the ice-albedo feedback in late summer. In statistics, the square of correlation coefficient can indicate the proportion of the variance in the dependent variable that is predictable from the independent variable [*Glantz and Slinker*, 1990]. Therefore, the declining trends of regional composite and sea ice albedos can explain the delayed timing of ice surface freezeup by 70% and 60%, respectively (Figures 7c and 7d).

3.4. Portioning of Surface Solar Radiation

Because the seasonal evolution of sea ice albedo has changed significantly since 2007, we used the data of CLARA albedo, ERA-reanalysis radiation, and SSM/I ice concentration averaged over 2007–2009 to characterize quantitatively the portioning of solar radiation over the surface of the ice-ocean system. The radiations reflected by the ice-ocean system (F_r) can be described as:

$$F_r = F_{in}(C_i\alpha_i + C_w\alpha_w), \tag{3}$$

where F_{in} is the incident radiation. The inputs of radiation to the open water (F_w) and sea ice (F_i) are:

$$F_w = F_{in}C_w(1-\alpha_w), \tag{4}$$

and

$$F_i = F_{in}C_i(1-\alpha_i). \tag{5}$$

We note that the input of radiation to the sea ice includes the radiation absorbed by sea ice and that transmitted into upper ocean through the ice cover. The incident solar radiation reached its annual maximum at the summer solstice, following which it declined gradually with time. In addition to seasonal change, incident solar radiation was also modulated by variations of cloud cover and it showed high daily variability. Although it had a similar seasonal behavior in all the subregions, the partition of the solar radiation at the surface into absorption (at surface and below) and reflection components showed distinct patterns from south to north (Figure 8). In all the subregions, the reflected radiation decreased gradually from June to August because of the decreases in insolation and the composite albedo. Although insolation was decreasing, the radiation absorbed by open water increased until the end of July and then remained stable to the

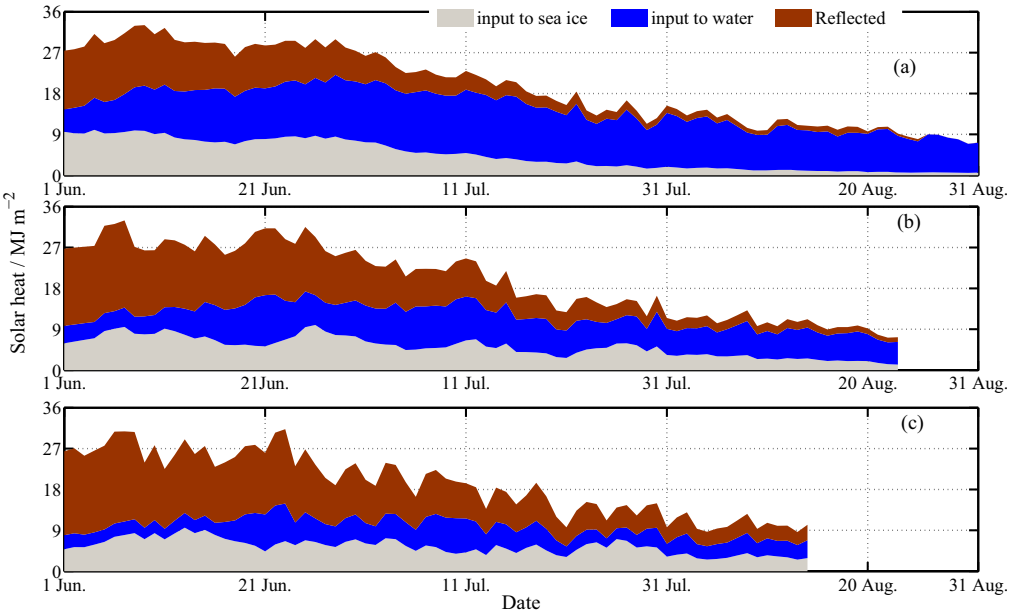

Figure 8. Seasonal evolution of daily inputs of solar radiation to sea ice and open water individually and daily radiation reflected by the composite surface averaged over 2007–2009 for the regions (a) 70°N–74°N, (b) 74°N–78°N, and (C) 78°N–82°N.

end of August, which can be attributed to the increase of the area of open water. In contrast, because the effect of ice area loss overwhelmed that of the decrease in ice albedo, the input of radiation to sea ice decreased distinctly from June to August in the region 70°N–74°N. However, in the region 78°N–82°N, the input of radiation to sea ice remained almost constant after the summer solstice. We infer that in this subregion, the effect of the decrease in ice area was counteracted by that of the decrease in ice albedo, in the case of the portioning of surface solar radiation, because less open water was produced there. Generally, solar radiation in the low latitudes was absorbed mainly by the open water, whereas in higher latitudes, it was absorbed mainly by melt ponds on the sea ice. This was consistent with the fact that the poleward decrease of ice bottom melt during summer was much larger than that of ice surface melt [*Perovich and Richter-Menge*, 2016].

During 1 June to 19 August, the long-term trend of the input ratio of radiation to open water over 1982–2009 was significant at the 99.9% confidence level because of the increase of the open water area (Figure 9). The linear trend indicated that this ratio has increased by about twofold from 18% to 35% over 28 years. In the summers of 2007 and 2008, because of the extreme anomalies of sea ice loss, the input ratios of radiation to open water were about 1.7 times the long-term 1982–2009 average. The linear trend indicated that the absorption ratio of radiation by the composite surface of sea ice and open water increased from 46% to 63% during 1982–2009. Correspondingly, the solar radiation absorbed by the composite surface during 1 June to 19 August increased from 751 to 1033 MJ·m^{-2} over these 28 years. The total increased solar heat input of 282 MJ·m^{-2} to the ice-ocean system can provide sufficient heat to potentially decrease the thickness of ice by about 1.03 m (assuming a latent heat of fusion of 0.3 MJ·kg^{-1} and a density of 910 kg·m^{-3} for sea ice in summer). In the same period, the ice concentration and ice albedo decreased from 80% to 60% and from 0.65 to 0.52, respectively. Setting the ice albedo equal to the long-term average of 0.6, the decrease in ice area implied an increase of solar heat input of 172 MJ·m^{-2}. Setting the ice concentration equal to the long-term average of 70%, a decrease of ice albedo implied an increase of solar heat input of 149 MJ·m^{-2}. Because the effects of loss of sea ice area and decreased sea ice albedo might cancel each other, the solar heat input to the sea ice remained stable during 1982–2009; its trend was insignificant at the 95% confidence level.

In June, the long-term average daily incident solar radiation in the study region was 28.2 MJ·m^{-2}. This value decreased to 20.0 and 10.6 MJ·m^{-2} in July and during 1–19 August, respectively. The linear trend during 1982–2009 indicated that the composite albedo decreased by 0.15, 0.15, and 0.23 in June, July, and 1–19

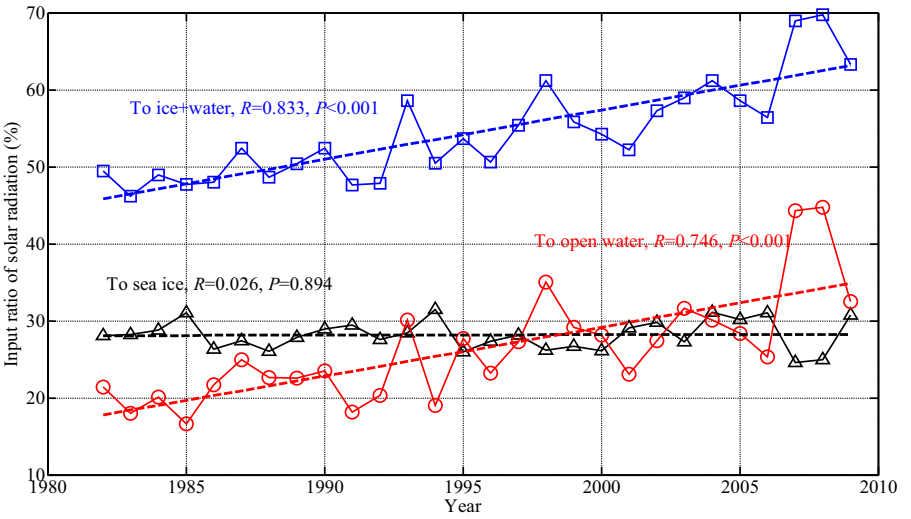

Figure 9. Long-term trends over 1982–2009 for the input ratios of solar radiation to sea ice and open water individually, and to the composite surface averaged during 1 June to 19 August; dashed lines denote the linear regression.

August, respectively. The decreased composite albedo resulted in an increase of daily solar radiation input to the ice-ocean system by 3.2, 1.6, and 1.7 MJ·m^{-2} in these three periods, respectively. Therefore, because of the distinct annual cycle of incident solar radiation, the sensitivity of the absorption of solar radiation to the changes in composite albedo was higher in early summer than in late summer.

4. Discussions

4.1. Influence of Atmospheric Circulation Pattern on Arctic Sea Ice-Albedo Feedback

The ice-albedo feedback focuses mainly on thermodynamics, however, sea ice motion in terms of advection and deformation plays an important role in opening and closing of sea ice [e.g., *Leppäranta*, 2011]. Sea ice dynamics are forced by winds and currents, which are mostly associated with atmospheric circulation patterns and mesoscale cyclones. Our study region is located upstream of the Transpolar Drift Stream (TDS) and, for the most part, it is within the Beaufort Gyre (BG). Thus, sea ice motion within this region can be influenced by both current systems. The intensities of the BG and TDS can be well explained by the two leading Arctic atmospheric circulation patterns, i.e., the AO and the DA [*Wang et al.*, 2009; *Lei et al.*, 2015, 2016].

A negative AO would enhance the advection of multiyear ice from north of the Canadian Arctic Archipelago to the study region because of anticyclonic wind anomalies [*Kwok et al.*, 2013]. However, the multiyear ice might melt completely or drift further into the East Siberian Sea during the summer. Therefore, the polarity of the AO cannot provide an inevitable linkage to the sea ice retreat within the study region during summer. There was no significant correlation between the summer AO index and regional ice concentration. In contrast, the correlations between the summer DA index and regional ice concentration or composite albedo were statistically significant at the 99.9% confidence level (Figures 10a and 10b). Under positive polarity of the DA, a greater amount of sea ice within the study region can drift northward and accumulate in the TDS system. Therefore, high positive polarity of the summer DA is related to reduced summer ice area and a lower composite albedo. Consequently, the open water absorbs more solar radiation, which then enhances the ice-albedo feedback. Even more interesting is that the correlation between the DA index and ice albedo in summer was significant at the 99.9% confidence level (Figure 10c). This implies that high positive polarity of the summer DA is related to more obvious ice surface melting, which could be attributed to that the prevailing southerly winds bringing relatively warmer air masses into the region. Furthermore, the warm open waters would in turn warm the overlying atmosphere. Both these two regimes result in an increase in Arctic surface air temperature [*J. Wang et al.*, 2014], which leads to increases in surface longwave radiation and in turbulent heat fluxes that introduce additional ice surface melting [*Zhang et al.*, 2008]. In two extreme years (2007 and 2008), the summer DA indices were >0.5. These high positive polarities were

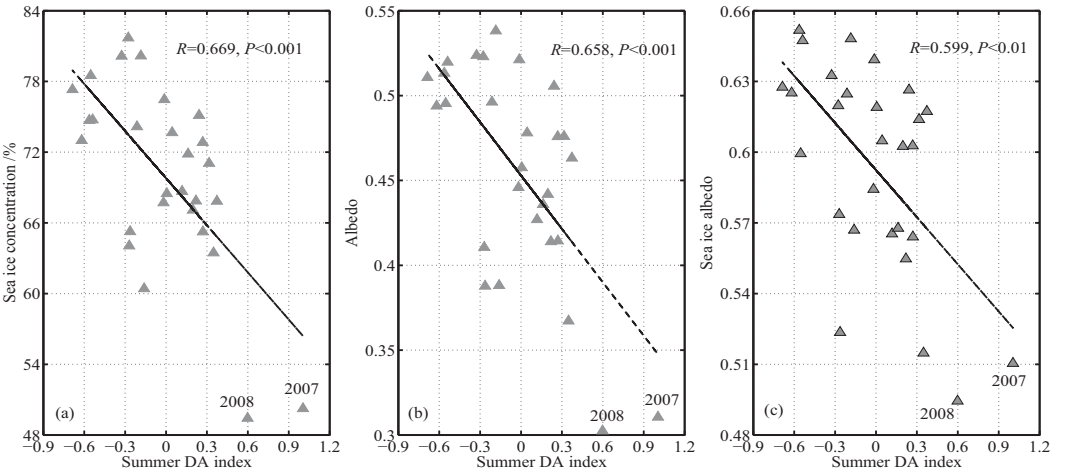

Figure 10. Linear regressions of ice concentration, composite albedo, and ice albedo in May–August against summer DA index in 1982–2009.

related to the lowest sea ice concentrations of 50% and 49%, regional composite albedos of 0.31 and 0.30, and ice albedos of 0.51 and 0.49 in 2007 and 2008, respectively. Synthetic analysis showed that the average ice concentration, regional composite albedo, and ice albedo under positive polarity of the DA (14 cases) were 66%, 0.42, and 0.57, respectively, all significantly lower than for negative polarity of the DA (14 cases), i.e., 74%, 0.48, and 0.61, respectively.

4.2. Limitations of the Data and Methods

The CLARA albedo data were available only until late August for the entire study region, which imposed the main limitation on the examination of the seasonal evolution of ice albedo, because information on the freezeup in early fall was unknown. This is not a trivial matter because albedo increases rapidly at that time, for both young ice and surviving multiyear ice. In addition, the CLARA albedo represents a clear-sky albedo. For the same surface, albedo can be influenced by external factors such as cloud fraction and solar zenith angle that change the incident solar spectrum [*Grenfell and Perovich*, 2008; *Wang and Key*, 2005]. The influence of solar zenith angle is unlikely to have any long-term trend. The cloud fraction in the regions north of 60°N increased from 74.3% to 75.4% during 1982–2004 [*Wang et al*., 2012]. The incident spectral irradiance weights the visible wavelength region more strongly compared with the infrared component on cloudy days. The wavelength-integrated albedo of sea ice is larger on cloudy days than on clear-sky days, with a difference of about 7% [*Grenfell and Perovich*, 1984]. Consequently, the increase of cloud fraction can induce a small increase in all-sky sea ice albedo based on the approximate calculation using equation (2) (about 0.0005 or 0.08% from 1982 to 2004), which can be neglected compared with the long-term decrease in clear-sky sea ice albedo (about 0.12 or 20% from 1982 to 2009). The long-term decreasing trend of clear-sky sea ice albedo can approximately equal to that of all-sky sea ice albedo. This approximate calculation suggests that changes in cloudiness only can play a negligible role in observed Arctic Ocean darkening.

The accuracy of the satellite-derived sea ice albedo depends mainly on the quality of the estimated ice concentration and composite albedo. During winter, sea ice concentration can be estimated to an accuracy of 2–5% from satellite passive microwave data [*Andersen et al*., 2007]. However, during the melt season, this accuracy decreases significantly because of the weakening of open water-ice contrasts. Compared with ship-based measurements, the root-mean-square error of the SSM/I BST ice concentration in Antarctica is about 15% in summer [*Beitsch et al*., 2015]. In the Arctic Ocean, melt ponds are very likely interpreted as open water by passive microwave measurements, while the area of ice between ponds is generally overestimated [*Kern et al*., 2016]. These two effects might partly cancel each other out. However, when the melt pond coverage reaches a certain threshold, the sea ice concentration would generally be underestimated by passive microwave measurements [*Andersen et al*., 2007; *Kern et al*., 2016].

To quantify the influence of uncertainty of ice concentration on the accuracy of the estimated ice albedo, we adjusted the ice concentration using an absolute increment of −5% to 10% for all pixels. The intention

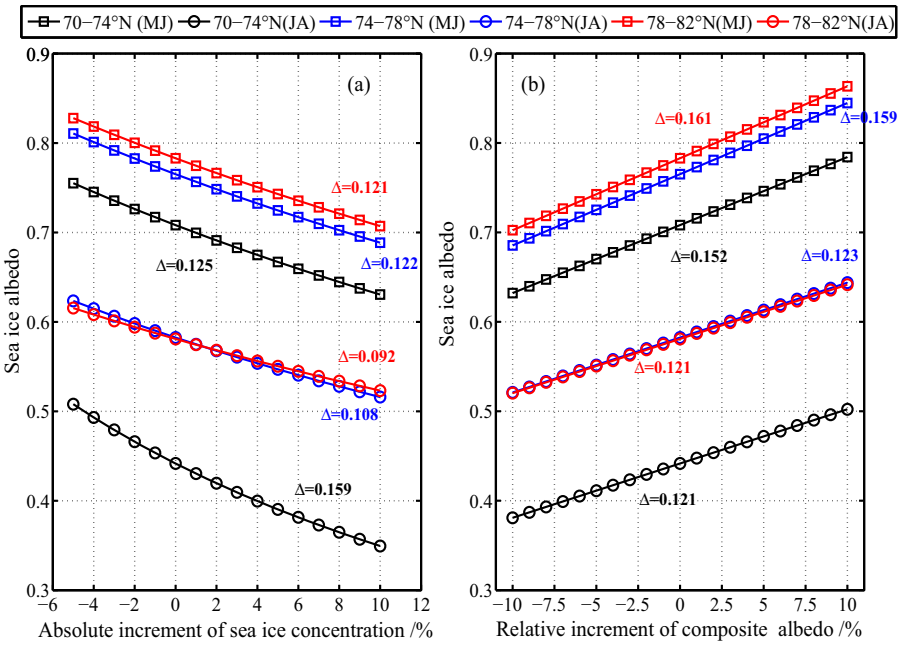

Figure 11. Variations of ice albedo (a) against increase of ice concentration related to the SMM/I observed value and (b) against relative increase of composite albedo related to the CLARA value. Also shown are the total deviations for the entire testing range.

was to compensate the potential underestimation of passive microwave measurements by using a wider range of positive change from the measurements. We found that underestimated sea ice concentration would result in overestimated sea ice albedo (Figure 11a). This effect would be enhanced with a decrease in ice concentration. The average sea ice concentration was lowest (39%) in the region 70°N–74°N in late summer (July–August). In this case, an increment of ice concentration from −5% to 10% resulted in the largest change in ice albedo of 0.159. In addition, the quality of the ice concentration product from passive microwave measurements is relatively poor in the MIZ because of large number of pixels that include mixed ice and water [*Spreen et al*., 2008]. Therefore, the influence of ice concentration on the accuracy of the estimated ice albedo would be furthermore strengthened. The overestimated ice albedo resulting from the underestimated ice concentration could partly explain why the satellite-derived ice albedo is generally larger than the SHEBA in situ data, when the melt pond fraction has reached its annual maximum.

The relative accuracy of the CLARA albedo, which is generally unbiased, is 5–15% [*Riihelä et al*., 2013b]. To perform a sensitivity analysis, we adjusted the albedo with relative increments from −10% to 10% for all pixels. An overestimated composite albedo would result in an overestimated ice albedo (Figure 11b). The sensitivity would also be enhanced with a decrease of ice concentration or an increase of regional composite albedo, while the latter influence was stronger. Therefore, the increase in sea ice albedo due to the overestimated composite albedo was larger in early summer than in late summer for all subregions.

Generally, an underestimation of ice concentration by 10% results in an overestimation of sea ice albedo by about 0.08 in early summer and by 0.06–0.10 in late summer. A relative uncertainty of 10% in the CLARA albedo results in an uncertainty of ice albedo of about 0.08 in early summer and 0.06 in late summer. Therefore, the estimated ice albedo based on the data and method of this study can be considered acceptable, because the seasonal range of ice albedo is generally 3–6 times these uncertainties. However, our estimated annual minimum ice albedo might be overestimated because of the false interpretation of melt ponds by the satellite measurements.

To estimate the portioning of surface solar radiation, we used the clear-sky CLARA albedo instead of the all-sky albedo. As mentioned above, overcast sea ice albedo is greater about 7% than the clear-sky albedo. For open water, whose albedo spectrum is essentially flat, the difference between overcast albedo and clear-sky albedo is negligible [*Grenfell and Perovich*, 2004]. In June–July from 1982 to 2009, the daily averages of incident radiation, sea ice concentration, and clear-sky ice albedo were 24.5 $MJ{\cdot}m^{-2}$, 78%, and 0.67,

respectively. Using the climatology of Arctic summer cloud fraction of 75% obtained from satellite observations during 1982–2004 [*Wang et al*., 2012], the all-sky ice albedo is estimated to be 0.035 larger than the clear-sky ice albedo. In June–July from 1982 to 2009, the daily average input of radiation to sea ice are 6.3 and 5.7 MJ·m^{-2}, and the daily reflected radiations by the composite surface of ice and water are 13.1and 13.7 MJ·m^{-2} for using the clear-sky ice albedo and all-sky ice albedo, respectively. Therefore, the relative uncertainty of the portioning of surface solar radiation is about 5–10% due to using clear-sky ice albedo instead of all-sky ice albedo.

5. Conclusions and Summary

Using the SSM/I BST ice concentration and CLARA black-sky albedo, the long-term trends and seasonal evolutions of sea ice concentration, regional composite albedo, and sea ice albedo were obtained. Based on the above investigations, the following conclusions were drawn.

All these variables showed significant negative long-term trends. The trend of sea ice loss was more significant in late summer than in early summer, whereas the trend of decrease in sea ice albedo was rather uniform. In July–August 1982–2009, linear trends of composite albedo and sea ice albedo were −0.069 and −0.046 units per decade, i.e., both about twice those of the entire Arctic Ocean. Thus, the study region could be considered as a critical area for the Arctic ice-albedo feedback.

The decrease in composite albedo was more related to the decrease in sea ice albedo in early summer, which could be explained by the early onset of ice surface melt, rather than the onset of sea ice loss. In contrast, in late summer, the loss of sea ice area has more profound impact on the composite albedo decrease, due to the large difference in the albedos of open water and sea ice. Both the seasonal evolution and the magnitude of the satellite-derived ice albedo were very close to those derived from the SHEBA data, supporting the reliability of the satellite-derived information. When melt pond fraction reached its annual maximum, the satellite-derived ice albedo was slightly larger than the average in situ value. This was partly attributed to the measurement scale and partly to the potential underestimation of ice concentration by the passive microwave measurements under the presence of melt ponds. At the SHEBA geolocations, an identifiable change in sea ice albedo has occurred since 2007, which can be explained by the replacement of multiyear ice by first-year ice as well as the delayed refreezing.

Comparison with the satellite-derived ice albedo confirmed that the parameterizations of sea ice albedo established on the basis of in situ measurements by *Perovich et al*. [2007a] and *Perovich and Polashenski* [2012] are applicable not only for floe scale but also for basin scale. However, the seasonal range of parameterized ice albedo should be adjusted for different regions because the intensities of ice surface melting and ponding are likely to have large spatial variability.

The ice-albedo feedback, which is one of the major contributors to Arctic Amplification, is more intense in late summer than in early summer because of the accumulated solar heat within the ice-ocean system. Therefore, the long-term delaying trend of ice surface freezeup was stronger than the trend of earlier onset of ice surface melt. Changing sea ice conditions within the study region resulted in an increase of the total solar heat input to the ice-ocean system by 282 MJ·m^{-2} during 1 June to 19 August from 1982 to 2009, providing enough heat to reduce ice thickness by about 1.03 m. This potential increase of ice melting is larger than the climatological ice surface melting (∼0.6 m) or ice bottom melting (∼0.8 m) in the Beaufort Sea [*Perovich and Richter-Menge*, 2016]. The positive DA would bring warmer air masses into the region and advects the ice northward out of the region. Although the Arctic ice-albedo feedback involves multiple complex processes [*J. Wang et al*., 2014] and the atmospheric circulation pattern is not the major cause for Arctic albedo change, the positive DA would enhance the ice-albedo feedback in the study region through strengthening the interactions between ice dynamics and thermodynamics.

Due to the limitation of availability of CLARA albedo data, sea ice albedo during the refreezing phase cannot be obtained. Therefore, the combination of satellite-derived albedo and the in situ measured albedo is very necessary. The unmanned observation combining one sea ice mass balance buoy and one spectral radiation buoy is a good tool to acquire the data of radiation-ice interactions during the entire melt season [e.g., *C. Wang et al*., 2014]. The maximum uncertainty of the ice albedo was estimated to be <0.16 resulting from the uncertainties of the products of sea ice concentration and composite albedo, which is much smaller

than the seasonal range. Therefore, the seasonal evolution of sea ice albedo found in this study is unambiguous. Clouds would increase sea ice albedo. Using the clear-sky ice albedo instead of all-sky ice albedo to estimate portioning of surface radiation, the relative uncertainty is about 5–10%. However, the corresponding uncertainty on long-term change is insignificant because the long-term change in summer Arctic cloudiness is very small.

Acknowledgments
This work was financially supported by grants from the National Natural Science Foundation of China (41476170), Chinese Polar Environment Comprehensive Investigation and Assessment Programs (CHINARE2016-03-01/04-03/04-04), and Chinese Arctic and Antarctic Administration (IC2014007). M.L. was supported by the Nordic Center of Excellence Cryosphere-Atmosphere Interactions in a Changing Arctic Climate (CRAICC). J.W. was supported by the NOAA CPO Office of Arctic Research through RUSALCA project (1821). L.K. was funded by the DFG (EXC177). We also wish to acknowledge CMSAF for providing CLARA-A1 albedo data, NSIDC for SSM/I ice concentration data, NASA Cryospheric Sciences Research Portal for sea ice melt data, ICDC of University of Hamburg for MODIS melt pond data, ECWMF for ERA-interim data, and NCEP for Reanalysis 2 data. The satellite-derived sea ice albedo is available from the authors on request (leiruibo@pric.org.cn).

References

Andersen, S., R. T. Tonboe, L. Kaleschke, G. Heygster, and L. T. Pedersen (2007), Intercomparison of passive microwave sea ice concentration retrievals over the high-concentration Arctic sea ice, *J. Geophys. Res.*, *112*, C08004, doi:10.1029/2006JC003543.

Arndt, S., and M. Nicolaus (2014), Seasonal cycle and long-term trend of solar energy fluxes through Arctic sea ice, *Cryosphere*, *8*(6), 2219–2233.

Beitsch, A., S. Kern, and L. Kaleschke (2015), Comparison of SSM/I and AMSR-E sea ice concentrations with ASPeCt ship observations around Antarctica, *IEEE Trans. Geosci. Remote Sens.*, *53*(4), 1985–1996.

Comiso, J. C. (2000), Bootstrap sea ice concentrations from Nimbus-7 SMMR and DMSP SSM/I-SSMIS, Version 2, daily sea ice concentration [updated 2015], NASA Natl. Snow and Ice Data Cent. Distrib. Active Arch. Cent., Boulder, Colo.

Eicken, H., T. C. Grenfell, D. K. Perovich, J. A. Richter-Menge, and K. Frey (2004), Hydraulic controls of summer Arctic pack ice albedo, *J. Geophys. Res.*, *109*, C08007, doi:10.1029/2003JC001989.

Glantz, S. A., and B. K. Slinker (1990), *Primer of Applied Regression and Analysis of Variance*, McGraw-Hill, N. Y.

Grenfell, T. C., and D. K. Perovich (1984), Spectral albedos of sea ice and incident solar irradiance in the Southern Beaufort Sea, *J. Geophys. Res.*, *89*, 3573–3580.

Grenfell, T. C., and D. K. Perovich (2004), Seasonal and spatial evolution of albedo in a snow-ice-land-ocean environment, *J. Geophys. Res.*, *109*, C01001, doi:10.1029/2003JC001866.

Grenfell, T. C., and D. K. Perovich (2008), Incident spectral irradiance in the Arctic Basin during the summer and fall, *J. Geophys. Res.*, *113*, D12117, doi:10.1029/2007JD009418.

Kern, S., A. Rösel, L. T. Pedersen, N. Ivanova, R. Saldo, and R. T. Tonboe (2016), The impact of melt ponds on summertime microwave brightness temperatures and sea ice concentrations, *Cryosphere Discuss.*, 1–54, doi:10.5194/tc-2015-202.

Kosaka, Y., and S. Xie (2013), Recent global-warming hiatus tied to equatorial Pacific surface cooling, *Nature*, *501*, 403–408.

Kwok, R., G. Spreen, and S. Pang (2013), Arctic sea ice circulation and drift speed: Decadal trends and ocean currents, *J. Geophys. Res. Oceans*, *118*, 2408–2425, doi:10.1002/jgrc.20191.

Lei, R., H. Xie, J. Wang, M. Leppäranta, I. Jónsdóttir, and Z. Zhang (2015), Changes in sea ice conditions along the Arctic Northeast Passage from 1979 to 2012, *Cold Reg. Sci. Technol.*, *119*, 132–144.

Lei, R., P. Heil, J. Wang, Z. Zhang, Q. Li, and N. Li (2016), Characterization of sea-ice kinematic in the Arctic outflow region using buoy data, *Polar Res.*, *35*, 22,658, 1–15, doi:10.3402/polar.v35.22658.

Leppäranta, M. (2011), *The Drift of Sea Ice*, 2nd ed., 347 pp., Springer-Praxis, Heidelberg, Germany.

Liu, J., Z. Zhang, J. Inoue, and R. M. Horton (2007), Evaluation of snow/ice albedo parameterizations and their impacts on sea ice simulations, *Int. J. Climatol.*, *27*, 81–91.

Lu, P., M. Leppäranta, B. Cheng, and Z. Li (2016), Dependence of melt pond albedo on pond depth and underlying ice properties, *Cold Reg. Sci. Technol.*, *124*, 1–10.

Markus, T., J. C. Stroeve, and J. Miller (2009), Recent changes in Arctic sea ice melt onset, freezeup, and melt season length, *J. Geophys. Res.*, *114*, C12024, doi:10.1029/2009JC005436.

Maslanik, J., J. Stroeve, C. Fowler, and W. Emery (2011), Distribution and trends in Arctic sea ice age through spring 2011, *Geophys. Res. Lett.*, *38*, L13502, doi:10.1029/2011GL047735.

Nicolaus, M., C. Katlein, J. Maslanik, and S. Hendricks (2012), Changes in Arctic sea ice result in increasing light transmittance and absorption, *Geophys. Res. Lett.*, *39*, L24501, doi:10.1029/2012GL053738.

Pegau, W. S., and C. A. Paulson (2001), The albedo of Arctic leads in summer, *Ann. Glaciol.*, *33*, 221–224.

Perovich, D. K., and C. Polashenski (2012), Albedo evolution of seasonal Arctic sea ice, *Geophys. Res. Lett.*, *39*, L08501, doi:10.1029/2012GL051432.

Perovich, D. K., and J. A. Richter-Menge (2016), Regional variability in sea ice melt in a changing Arctic, *Philos. Trans. R. Soc. A*, *373*, 2045–2057.

Perovich, D. K., T. C. Grenfell, B. Light, and P. V. Hobbs (2002), Seasonal evolution of the albedo of multiyear Arctic sea ice, *J. Geophys. Res.*, *107*(C10), 8044, doi:10.1029/2000JC000438.

Perovich, D. K., S. V. Nghiem, T. Markus, and A. Schweiger (2007a), Seasonal evolution and interannual variability of the local solar energy absorbed by the Arctic sea ice–ocean system, *J. Geophys. Res.*, *112*, C03005, doi:10.1029/2006JC003558.

Perovich, D. K., B. Light, H. Eicken, K. F. Jones, K. Runciman, and S. V. Nghiem (2007b), Increasing solar heating of the Arctic Ocean and adjacent seas, 1979–2005: Attribution and role in the ice-albedo feedback, *Geophys. Res. Lett.*, *34*, L19505, doi:10.1029/2007GL031480.

Perovich, D. K., K. F. Jones, B. Light, H. Eicken, T. Markus, J. Strieve, and R. Lindsay (2011), Solar partitioning in a changing Arctic sea-ice cover, *Ann. Glaciol.*, *52*(57), 192–196.

Pistone, K., I. Eisenman, and V. Ramanathan (2014), Observational determination of albedo decrease caused by vanishing Arctic sea ice, *Proc. Natl. Acad. Sci. U. S. A.*, *111*(9), 3322–3326.

Pithan, F., and T. Mauritsen (2014), Arctic amplification dominated by temperature feedbacks in contemporary climate models, *Nat. Geosci.*, *7*(3), 181–184.

Riihelä, A., T. Manninen, V. Laine, K. Andersson, and F. Kaspar (2013a), CLARA-SAL: A global 28-yr timeseries of Earth's black-sky surface albedo, *Atmos. Chem. Phys.*, *13*, 3743–3762.

Riihelä, A., T. Manninen, and V. Laine (2013b), Observed changes in the albedo of the Arctic sea-ice zone for the period 1982–2009, *Nat. Clim. Change*, *3*, 895–898.

Rösel, A., and L. Kaleschke (2012), Exceptional melt pond occurrence in the years 2007 and 2011 on the Arctic sea ice revealed from MODIS satellite data, *J. Geophys. Res.*, *117*, C05018, doi:10.1029/2011JC007869.

Rösel, A., L. Kaleschke, and G. Birnbaum (2012), Melt ponds on Arctic sea ice determined from MODIS satellite data using an artificial neural network, *Cryosphere*, *6*, 431–446, doi:10.5194/tc-6-431-2012.

Schröder, D., D. L. Feltham, D. Flocco, and M. Tsamados (2014), September Arctic sea-ice minimum predicted by spring melt-pond fraction, *Nat. Clim. Change*, *4*, 353–357, doi:10.1038/nclimate2203.

Screen, J. A., and I. Simmonds (2010), The central role of diminishing sea ice in recent Arctic temperature amplification, *Nature*, *464*, 1334–1337, doi:10.1380/nature09051.

Serreze, M., and R. Barry (2011), Processes and impacts of Arctic Amplification, *Global Planet. Change*, *77*, 85–96.

Spreen, G., L. Kaleschke, and G. Heygster (2008), Sea ice remote sensing using AMSR-E 89 GHz channels, *J. Geophys. Res.*, *113*, C02S03, doi:10.1029/2005JC003384.

Timco, G. W., and M. E. Johnston (2002), Sea ice strength during the melt season, in *Proceedings of the 16th IAHR International Symposium on Ice*, vol. 2, pp. 187–193, Otago University, Dunedin, New Zealand.

Wang, C., M. A. Granskog, S. Gerland, S. R. Hudson, D. K. Perovich, M. Nicolaus, T. I. Karlsen, K. Fossan, and M. Bratrein (2014), Autonomous observations of solar energy partitioning in first year sea ice in the Arctic Basin, *J. Geophys. Res. Oceans*, *119*, 2066–2080, doi:10.1002/2013JC009459.

Wang, C., M. A. Granskog, S. R. Hudson, S. Gerland, A. K. Pavlov, D. K. Perovich, and M. Nicolaus (2016), Atmospheric conditions in the central Arctic Ocean through the melt seasons of 2012 and 2013: Impact on surface conditions and solar energy deposition into the ice-ocean system, *J. Geophys. Res. Atmos.*, *121*, 1043–1058, doi:10.1002/2015JD023712.

Wang, J., and M. Ikeda (2000), Arctic oscillation and Arctic sea-ice oscillation, *Geophys. Res. Lett.*, *27*, 1287–1290.

Wang, J., J. Zhang, E. Watanabe, K. Mizobata, M. Ikeda, J. E. Walsh, X. Bai, and B. Wu (2009), Is the dipole anomaly a major driver to record lows in the Arctic sea ice extent?, *Geophys. Res. Lett.*, *36*, L05706, doi:10.1029/2008GL036706.

Wang, J., H. Eicken, Y. Yu, X. Bai, J. Zhang, H. Hu, D.-R. Wang, M. Ikeda, K. Mizobata K., and J. E. Overland (2014), Abrupt climate changes and emerging ice-ocean processes in the Pacific Arctic region and the Bering Sea, in *The Pacific Arctic Region: Ecosystem Status and Trends in a Rapidly Changing Environment*, edited by J. M. Grebmeier and W. Maslowski, pp. 65–100, Springer, Dordrecht, Netherlands.

Wang, X., and J. R. Key (2005), Arctic surface, cloud, and radiation properties based on the AVHRR polar pathfinder dataset. Part I: Spatial and temporal characteristics, *J. Clim.*, *18*, 2558–2574.

Wang, X., J. R. Key, Y. Liu, C. Fowler, J. Maslanik, and M. Tschudi (2012), Arctic climate variability and trends from satellite observations, *Adv. Meteorol.*, *2012*, 1–22.

Webster, M. A., I. G. Rigor, D. K. Perovich, J. A. Richter-Menge, C. M. Polashenski, and B. Light (2015), Seasonal evolution of melt ponds on Arctic sea ice, *J. Geophys. Res. Oceans*, *120*, 5968–5982, doi:10.1002/2015JC011030.

Xia, W., H. Xie, and C. Ke (2014), Assessing trend and variation of Arctic sea ice extent during 1979-2012 from a latitude perspective of ice edge, *Polar Res.*, *33*, 21,249, 1–13, doi:10.3402/polar.v33.21249.

Zhang, J., R. Lindsay, M. Steele, and A. Schweiger (2008), What drove the dramatic retreat of arctic sea ice during summer 2007?, *Geophys. Res. Lett.*, *35*, L11505, doi:10.1029/2008GL034005.